Fe□O□@Polydiallyl Isophthalate Magnetic Microspheres for Enhanced MRI/CT and Magnetothermal Effect-Guided Tumor Ablation

Piaoyi Chen
Guangzhou Medical University
Yanfang Zhou
Guangzhou Medical University
Mianrong Chen
Guangzhou Medical University Second Affiliated Hospital
Yingying Lun
Guangzhou Medical University
Qiuxia Li
Guangzhou Medical University
Qinglin Xiao
Guangzhou Medical University
Yugang Huang
Guangzhou Medical University
Jiesong Li
Guangzhou Medical University
Guodong Ye (gzhygd@gzhmu.edu.cn)
Guangzhou Medical University https://orcid.org/0000-0002-7202-0006

Research article

Keywords:

Posted Date: April 11th, 2022

DOI: https://doi.org/10.21203/rs.3.rs-1531392/v1

Abstract

Background: Multi-functional embolic microspheres for treating stage B hepatocellar carcinoma often require complex synthesis processes and harsh conditions. But the traditional embolic agents (e.g. polyvinyl alcohol and iodized oil) often cause unexpected embolism and have potential risks of damaging the human body. The aim of this research was to use a photo-click method to prepare multifunctional microspheres with magnetocaloric effect and MR/CT/DSA imaging function used in the transcatheter arterial embolization.

Methods: Fe_3O_4@polydiallyl isophthalate (Fe_3O_4@PDAIP) magnetic microspheres were synthesized by one-pot photopolymerization without hindered by degradative chain transfer. The in vitro and in vivo anti-tumor effects were characterized with hepatoma cell experiments and tumor-bearing mouse model. The DSA and CT in vitro were utilized to evaluate imaging ability of Fe_3O_4@PDAIP. The safe was tested *via* histopathological examination and serum detection.

Result: The results showed that Fe_3O_4@PDAIP magnetic microspheres had ablation effect on tumor cells and had imaging effect through MR/CT/DSA scanning. The microspheres was heated to 42-48 ^oC by magnetocaloric effect in alternating magnetic field, which significantly decreased the activity of mouse liver cancer cells in vitro. In vivo, it can inhibit the growth of tumor after magnetothermal therapy without obvious toxicity.

Conclusion: Fe_3O_4@PDAIP magnetic microspheres can be potentially applied to the locoregional and precise interventional treatment of liver tumors.

1. Background

Liver cancer has been recognized as one of the leading causes of mortality worldwide for decades. However traditional chemotherapies often were accompanied by irreversible damage for normal tissue due to its lack of selectivity for tumor tissue alone. Thus, transcatheter arterial embolization (TAE) including transcatheter arterial chemoembolization (TACE) [1–3] is a superior method in treatment of tumors, which use microspheres often be loaded with drugs [4–6], radioactive material such as Y^{90}[7–9]. Besides, Cu, Gd, Au and others are heated being exposed to near-infrared laser apply to photothermal therapy [10–13]. But the harsh synthetic conditions of radioactive microspheres [14, 15] and the physical constrains of near infrared light penetration through tissue (< 1cm)[16] make the clinical performance unsatisfactory.

Magnetothermal therapy utilizes deeper penetration capability of magnetic field to activate magnetic response materials and generate hyperthermia to ablate tumors under the high-frequency alternating magnetic field (AMF) [17]. Thus, the treatment is localized to target spot, so the patient's body is subjected only to a small, focused field, minimizing the possibility of side effects. At present, the most widely reported magnetic microspheres are all most core/shell structure [18–20]: with a high molecular

polymer as the core, e.g. polyvinylbenzene, the nano-magnetic material is adsorbed by electrostatic adsorption and other forces, and then fixed by encapsulation[21]. But this layer-by-layer assembled structure often requires multi-step reaction that takes a long time to react or/and need a high temperature. Luckily, photopolymerization of allyl monomers proceeds without hindered by the well-known degradative chain transfer (DCT) under [3 + 2] photoinduced radical-mediated cyclization [22, 23], and then it has been found that stable and uniform microspheres can be formed by suspension polymerization for arterial embolization, which have been reported in our laboratory[24]. Therefore, we speculate that magnetic microspheres can be prepared by one-step reaction of allyl monomers to avoid the tedious synthesis steps like the multilayer microsphere. However, conventional allyl hydrophobic monomers cannot well disperse magnetic nanomaterials in microspheres. Thus, monomers used in magnetic microspheres often require [25]. But modified diallyl isophthalate monomers enable magnetic nanoparticles to be encapsulated in polymers by *cation*-π or polar interaction [26–28]. The interaction occurs when Fe in the edge of inorganic substance react with matrix of isophthalate. Besides, photoclick preparation occurs at room temperature and will not cause the magnetic material to lose its magnetism due to excessive temperature. Thus, we successfully synthesized Fe_3O_4@PDAIP magnetic microspheres based on design. Our aim is that magnetocaloric effect can be used in thermotherapy of tumors, and has embolization function, which can be applied to treat cancer synergistically. Moreover, Fe_3O_4@PDAIP magnetic microspheres were capable of being visualized on digital subtraction angiography (DSA), computerized tomography (CT), or magnetic resonance imaging (MRI) examinations. This can be used to track treatment progress.

2. Materials And Methods

2.1 Materials

2-Hydroxy-2-methyl-1-phenyl-1-propanone (HMPP) was purchased from Aladdin Reagent Co., Ltd. (Shanghai, China). Dially isophthalate (DAIP) and nano-Fe_3O_4 were purchased from Macleans Biochemical Technology Co., Ltd. (Shanghai, Chian). Polyvinyl pyrrolidone (PVP) was purchased from Aladdin Reagent Co., Ltd. (Shanghai, China). H_{22} mouse hepatoma cells were supplied by Wuhan University (Hubei, China). Pen-strep solution, phosphate buffered saline (PBS Gibco™), dulbecco's Modified Eagle Medium (DMEM Gibco™) and fetal bovine serum (FBS, Gibco™) were purchased from Thermo Fisher Scientific Biological Chemical Products Co. Ltd. (Beijing, China). Live & dead cell viability/cytotoxicity assay kit, i.e. calcein acridine orange (AO) and propidium iodide (PI), were obtained from Bestbio (Shanghai, China). Cell counting kit-8 (CCK-8) was obtained from Glpbio Technology (California, USA). SPF female Kunming mice (4 weeks old, 16 ~ 20g) were purchased from Guangdong Medical Experimental Animal Center (Guangdong, China). Sodium pentobarbital was purchased from Sigma, USA.

2.2 Synthesis of Fe_3O_4@PDAIP Magnetic Microsphere

The magnetic microspheres were synthesized on the basis of the work previously reported by Zhao[24]. 5wt% (0.1g) of PVP was added to 80mL H_2O under mechanical stirring at 600 revolutions per minute. 15wt% (0.3g) HMPP was mixed uniformly with 2g DAIP by ultrasonic treatment for 5 minutes. Then 4wt% nano-Fe_3O_4 (0.08g) was added and maintaining ultrasonic treatment for 4 minutes, the hydrophobic magnetic fluid with good dispersion was obtained. The magnetic fluid was slowly added to the above solution subsequently to form a water-oil mixture, the mixture was irradiated with an industrial middle-pressure mercury lamp (light intensity: 42mW/cm^2; wavelength: 365nm) for 60 minutes under stirring, finally yielded the nano-Fe_3O_4 modified polydiallyl isophthalate magnetic microspheres (Fe_3O_4@PDAIP). The microspheres were washed with distilled water, transferred to a dialysis bag. Then they were dialyzed for 48 hours and freeze-dried for 24 hours. Polydially isophthalate (PDAIP) microspheres were synthesized following the same method just without nano-Fe_3O_4. The route was shown in scheme 1.

2.3 Characterization of Fe_3O_4@PDAIP Microsphere

2.3.1 Morphological characterization

The morphology of Fe_3O_4@PDAIP magnetic microspheres was observed with a fluorescence microscope (Eclipse Ni-U, Nikon, Japan). The average size of the magnetic microspheres was determined using image software. At least 300 microspheres were counted and used to make a microsphere size distribution map. Elemental analysis of Fe_3O_4@PDAIP magnetic microspheres was carried out on a scanning electron microscope energy dispersive spectrometer (SEM/EDS, Phenom-ProX, Phenom-World, Holland).

2.3.2 Magnetic test

The vibrating sample magnetometer (VSM, LakeShore 7404) was used to test the hysteresis loop and the amplification of the low magnetic field area to determine the coercivity and remanence. The test setups were fast scanning (25 ~ 30Oe/s) with 30.44mg Fe_3O_4@PDAIP at 30 ^oC, the magnetic field range is ± 1T, and the scanning points are 500 points.

2.3.3 Infrared spectra (IR) analysis and thermal analysis

Fe_3O_4, PDAIP microspheres and Fe_3O_4@PDAIP magnetic microspheres was mixed with dry potassium bromide separately and determined by infrared spectroscopy (Nicolet 6700, Thermo Fisher Scientific, US) in the wave number scanning range of 4000-400cm^{-1}. Synchronous thermal analyzer (STA 449 F5 Jupiter, Netzsch, Germany) was used for thermal analysis under 50–800 ^oC (heating rate 20 ^oC/min), 20mL·min^{-1} N_2 atmosphere. 25mg sample is used to obtain thermogravimetric (TG) curve.

2.3.4 Study on Fe_3O_4@PDAIP magnetic microsphere stability.

Immerse 10/20/30mg of microspheres in 1mL of H_2O, PBS, and DMEM solutions, respectively, and observe their heating performance and particle size after 1, 2, and 7 days.

2.4 In vitro test

2.4.1 Heating performance of Fe_3O_4@PDAIP magnetic microspheres with or without cells

The high-frequency heating machine (Guangdong Taiguan Power Technology Co., Ltd. 15kW) was used for the heating test. The 350mm petri dishes were loaded with 10/20/30mg of Fe_3O_4@PDAIP magnetic microspheres respectively. Three parallel experiments were set in each group. The empty dish was used as a blank control, and turn on machine for 180s.

Add 1mL of H_{22} cells ($4 \sim 5 \times 10^5 mL^{-1}$) to a 350mm petri dish with the same dose of the microspheres above, and set up a control group (microspheres-free). The heating operation is the same as previous. The temperature is measured by thermal infrared imager (Testo 871, Testo SE & Co. KGaA, Germany).

2.4.2. Tumor cell survival with Fe_3O_4@PDAIP magnetic microspheres in AMF and cytotoxicity test.

H_{22} cells were cultured in 350mm petri dish (DMEM with 10% FBS and 1% pen-strep solution, 37 ^oC, 5% CO_2) for 24 hours, and the cell density was $4 \sim 5 \times 10^5 mL^{-1}$. 1mL microspheres with a concentration of 10/20/30mg·mL^{-1} were added respectively, and cultured for 24 hours continuously, then in the AMF for 180s. The microspheres were separated with magnets, and the cells were transferred into a 96-well plate with 100μL per well. After 24 hours, cells were incubated with 10μL of CCK-8 in medium for 2 hours in the dark at 37 ^oC. Blank group is pure media and control group is media incubated without magnetocaloric substance, the same below.

The cytotoxicity test, soaking 10/20/30 mg of microspheres in 1mL PBS for 3 days, the microspheres were separated to obtain the extract of the microspheres. The cells (100μL per well) were cultured to the same concentration by the above method and transferred to 96-well plates. After 24 and 48 hours, cells were incubated with 10μL of CCK-8 in medium for 2 hours in the dark at 37^oC, respectively. Six parallel experiments were set up for all groups in the above experiments. The optical densities (OD) were measured by microplate reader (Epoch, BioTek, US) at wavelength 450nm. Relative cell viability [29] was calculated using the following formula:

$$Relativecellviability(\%) = \frac{OD_{experiment} - OD_{blank}}{OD_{control} - OD_{blank}} \times 100\% (1)$$

2.4.3. Fluorescent staining of live & dead cell

According to the above scheme, the cells were cultured to 4 ~ 5 × $10^5 mL^{-1}$ in 350mm petri dish, and the magnetic magnetocaloric treatment was carried out by the same method. Finally, the microspheres and cell fluid were separated by magnets. The dye solution was configured according to the instructions of the commercial AO/PI kit. The above cells were washed twice with PBS, mixed evenly with 500mL staining solution and incubated at 4°C for 20 minutes in dark, then wash the cells with PBS [30, 31]. The staining was observed at 525nm (living cells, green) and 600nm (dead cells, red) wavelengths respectively by fluorescence microscope.

2.4.3. In vitro MRI/DSA/CT of Fe_3O_4@PDAIP magnetic microspheres

The agar solution with a concentration of 1% was transferred to a six-well plate while it was hot. 10/20/30mg of magnetic microspheres were added to the three wells and mixed evenly with agar [32], and the other three as blank controls. The MR imaging study was conducted using a MR imaging system (Philips). In field strength 3T, using T1 weighted imaging.

The DSA an CT visualization experiment was divided into four groups: Fe_3O_4; Fe_3O_4(4wt%)@PDAIP microspheres; Fe_3O_4(2wt%)@PDAIP microspheres and Fe_3O_4(0wt%)@PDAIP microspheres. Each group weighed 0.25g, 0.5g, 0.75g, respectively, into a 5mL EP tube, added 1mL of deionized water, and took images using a DSA machine (Siemens) at 52kV, 3mAs, DFOV 27.3cm × 27.3cm. The CT images are obtained by CT scanning (Philips) with 120kV, 150mAs and SW 1mm.

2.5 In vivo test

2.5.1 H_{22} tumor-bearing mouse model

H_{22} cells were grown to a density of 1 × $10^7 mL^{-1}$ in 1000mm medium using the above method. The tumor cells were injected in 12 mice subcutaneously at the junction of the chest and the right limb with a dose of 0.3mL. Put it in the environment of 25°C and 70% humidity for 48 hours and measure the length and width of the tumor. At the same time, the body weight of mice was recorded every two days.

2.5.2 Inhibitory effect of Fe_3O_4@PDAIP magnetic microspheres on tumor growth

1 mL of microspheres with a concentration of 10/20/30mg/mL was injected into the tumor site in multiple doses (about 0.3mL per injection) and 1mL PBS was injected as the control group. After 24 hours, the 3 mice/group was exposed to 180s in AMF and treated every 24 hours for a total of three times. The length and width of the tumor were measured every 2 days for a total of 14 days. The volumes of tumor were calculated according to the following formula [33]:

$$Tumorvolume\left(mm^3\right) = 0.52 \times length \times width^2 (2)$$

The mice containing microspheres and the PBS control group were placed in the MRI as mentioned above, and angiographic ability of magnetic microspheres was observed.

2.5.3 Detection of liver and kidney function

At the 14th day, the mice were anesthetized by an abdominal subcutaneous injection of 3wt% pentobarbital sodium at 0.05mL. After the mice were completely anesthetized, the eyeballs of the mice were removed and the blood was taken, centrifuged, and the supernatant was collected. The parameters are set as follows: centrifugal temperature 4 ^{o}C, 5000 revolutions per minute for 20 minutes. Serum indicators include alanine aminotransferase (ALT) and aspartate aminotransferase (AST) as liver function signals, blood urea nitrogen (BUN) and creatinine (CREA) as renal function signals.

2.5.5 Histopathological examinations

Tumor and heart, liver, spleen, lung and kidney were collected after dissection and fixed in 10% formalin solution, then processed and embedded in paraffin, and finally sliced by microtome. The pathologic organ changes were investigated using hematoxylin and eosin (H&E) staining [34]. Assess the degree of tumor cell necrosis and the inflammatory response of various organs.

3. Result

3.1 Morphological characterization

Under the fluorescence microscope, the particle size distribution of the microspheres was randomly selected to observe and calculate the size distribution of the microspheres, as shownin Fig. 1a. The particle size distribution is 20–145μm with average particle size 74μm. It shows a positive skew distribution, indicating that the magnetic microspheres have a wide particle size distribution. After photopolymerization, magnetic microspheres of different sizes can be further separated by classification and screening, which can occlude blood vessels of different calibers and flows to meet the needs of vascular embolization in different parts.

3.2 Spectral and thermal analysis

The TG curves of nano-Fe_3O_4, PDAIP microspheres and Fe_3O_4@PDAIP magnetic microspheres were measured. Figure 1b shows that nano-ferric oxide can remain stable without mass loss from 50 to 800^{o}C. The microspheres loaded with or without nano-ferric oxide began to decompose at about 400^{o}C, but the final residual mass of the magnetic microspheres indicated that the samples was loaded with 10wt% of ferric oxide higher the reactant ratio 4wt%. The fluctuation in loading might be attributed to the inevitable aggregation of magnetic nano-Fe_3O_4, or unreactive monomers lost.

The IR spectra of nano-Fe_3O_4, PDAIP and Fe_3O_4@PDAIP magnetic microspheres are shown in Fig. 1c. It shows that the peak of Fe_3O_4 at 586cm^{-1} and the increase in absorbance of Fe_3O_4@PDAIP magnetic microsphere around 580cm^{-1} is attributed to the Fe-O bond[35], which indicates that Fe_3O_4 was

successfully doped in Fe_3O_4@PDAIP magnetic microspheres. Peak 1729cm^{-1} is related to the C = O stretching vibration of the ester bond. It can be seen that the magnetic microspheres were successfully synthesized from DAIP monomer.

3.3 SEM-EDS analysis

The SEM images of the microsphere are shown in Fig. 1d. Spectral scan in a randomly selected area of microspheres in the Fig. 1e was used for elemental analysis. The results shown in Fig. 1f indicated the presence of three elements, carbon, oxygen, iron, in the microspheres, in line with the expected composition.

3.4 Magnetic test

The magnetic microspheres in the water are randomly dispersed in the water without or with a magnetic field (Fig. 2a), and under the action of magnetic field, they obviously accumulated in the direction of the magnetic field. VSM magnetic strength curve (Fig. 2b) showed that Fe_3O_4 did not lose magnetism after photopolymerization, which suggested that the Fe_3O_4@PDAIP had favorable magnetic response.

3.5 Thermal effect of Fe_3O_4@PDAIP magnetic microspheres and MRI/CT/DSA imaging

The temperature records of microsphere under AMF are shown in Fig. 3a (without cells) and 3b (with cells). The thermal effect caused by coil is excluded by the control group (gray line). The temperature can reach about 45 ~ 52^oC and 44 ~ 48^oC, respectively as the dose of microspheres increases from 10 to 30mg. In clinic, when tissues are heated to 41^oC, heat shock proteins can be upregulated as the defensive mechanisms for cells against thermal damage; whereas the irreversible cell necrosis occurs when the tissue temperature exceeds 42^oC. Moreover, cells death can occur rapidly owing to the vessel thrombosis and ischaemia at 46 ~ 52^oC [16]. Figure 3c show typical thermal infrared images of the temperature rise of Fe_3O_4@PDAIP *in vitro* and *in vivo*. It can be seen that the microspheres in the coil were obviously warmed up due to the magnetocaloric effect, and the tumor site in mice showed the similar result.

The MRI capabilities of magnetic microspheres *in vitro* and *in vivo* were presented in Fig. 3d. Compared with the MRI image of pure agar, the signal of microspheres in agar has changed obviously, and the distribution of the microsphere could be seen clearly. Similarly, the MRI images of the injected microspheres in mice also changed significantly compared with the control group, and the shadow area increased with the increase of microsphere dose. The DSA (left) and CT (right) images were showed in Fig. 4. It can be seen that the microspheres and deionized water cannot be clearly distinguished at 0wt% Fe_3O_4 content, but when the Fe_3O_4 content increased to 2wt% or 4wt%, the obvious boundary between the microspheres and water was found. Compared with the image of iron without microspheres embedded, the capability imaging of DSA is only related to the iron concentration. CT images indicate that the visualization ability of Fe_3O_4@PDAIP microspheres in CT scanning is parity with Fe_3O_4. These results

suggest that the Fe_3O_4@PDAIP magnetic microspheres have good capabilities on heating and MRI/CT enhanced imaging, and simultaneously have enormous potential in DSA imaging.

3.6 Fe_3O_4@PDAIP magnetic microspheres stability experiment

The stability of the microspheres immersed in different media (H_2O, PBS, DMEM) for 1, 2 and 7 days was investigated. As shown in Fig. 5a, the microspheres still had similar heating performance as Fig. 3a and 3b, they can even reach more than 40^oC at a low concentration. A significant correlation of the temperature and concentration was found. In Fig. 5b, the particle size distribution was measured by the previous method. The particle size distribution was 25 ~ 180μm (1 day), 40 ~ 200 μm (2 days), 35 ~ 180 μm (7 days) respectively. The average particle size was respectively 95.19μm (1 days), 101.95μm (2 days), 91.89 μm (7 days). Slight differences in particle size distribution and average were due to random sampling. These data indicate that the microspheres can still maintain their performance and morphology for a long time in different media without decomposition. This seems to be beneficial to a long-term embolization, and can greatly reduce the frequency of medication used by patients.

3.7 Cytotoxicity of Fe_3O_4@PDAIP magnetic microspheres

The CCK-8 assay (Fig. 6a) quantitatively showed that there was a slight negative influence on cell growth compared to the control group when the cells were co-cultured with Fe_3O_4@PDAIP extract of different concentrations for 1, 2 days, respectively. However, cell viabilities in these experimental groups were still above 80%. According to the toxicity grading guide, the Fe_3O_4@PDAIP cell toxicity was included in Grade I, representing relative growth rate between 75% and 99% during the culture process [36].

3.8 Inhibitory effect on tumor cells in vitro and in vivo.

After the cells containing different concentrations of microspheres were placed in AMF for 180s, the relative cell viabilities were determined by the CCK-8 assay. The results are shown in Fig. 6b. At a low concentration (10mg/mL), the tumor cells still maintained about 70% relative cell viability after experiencing the thermal effect of microspheres. When the concentration increased to a medium concentration (20mg/mL) and a high concentration (30mg/mL), the cell viability decreased significantly, only 50% compared with the control group. In addition, these cells were continuously observed. In the absence of microspheres or in a low concentration, the cell sap turned yellow within 24 hours, while cell sap of the middle and high concentration remained purplish red like the culture medium for 14 days or more. It implies that the metabolism of tumor cells has been affected by the thermal effect of middle and high concentration microspheres. Tumor size and body weight within 14 days are recorded in Fig. 6c and 6d. Similar results were obtained with the *in vitro* experiments. Tumor size was maintained or decreased over 14 days, in stark contrast to the control and low-concentration groups. The result of fluorescent staining of live & dead cell is shown in Fig. 6e. The higher the concentration of microspheres, the greater

the proportion of cancer cells apoptosis. The results of H&E staining (Fig. 6f) also showed that in the high concentration group, a large part of the H_{22} cells (blue-purple) were replaced by connective tissue (pink), confirming the obvious necrosis of tumor cells. Subcutaneous solid tumors in mice were collected after 14 days, as shown in Fig. 6g. The three parallel experiments show that microspheres of medium and high concentrations can significantly inhibit tumor growth *in vivo*. Besides, there is no noticeable change on the body weight of the mice (Fig. 6d). It is suggested that the Fe_3O_4@PDAIP magnetic microspheres have no visible damage to the body.

3.9 Histopathological examination and serum detection.

After 14 days, the heart, liver, spleen, lung and kidney of the experimental mice were collected and stained with H&E to make histopathological sections. These pictures are listed in Fig. 7a. The shape of cardiomyocytes is normal; the distribution of cells around the central hepatic vein was radial, and there was no obvious inflammatory cell infiltration; in spleen, there was no significant expansion of white pulp and no lymphocyte filling; in lung, with many cavity areas, there is no obvious congestion in the pulmonary vessels; and no obvious pathological changes in renal corpuscles and renal tubules. This means that all tumor-bearing mice showed no significant inflammation or lesions and their various organs functions are basically normal. Figure 7b showed the serum test results of liver and kidney function after 14 days. The normal ranges of the liver function indexes ALT and AST are 10.06 ~ 96.47U/L and 36.31 ~ 235.48U/L respectively. The normal indexes BUN and CREA of kidney are 10.81 ~ 34.74mg/dL and 10.91 ~ 85.09μmol/L[37, 38]. The results showed that the liver and kidney functions were within the normal range, indicating Fe_3O_4@PDAIP magnetic microspheres have good biocompatibility. Combining with the result of histological observation, it shows Fe_3O_4@PDAIP magnetic microspheres have equivalence or non-inferiority tumor ablation effect.

4. Discussion

In the past, blank microspheres only used for embolized blood vessels, but their clinical effects were not satisfactory, which often led to tumor recurrence and metastasis. Now more studies are focused on multi-functional microspheres. Microspheres containing nanomaterials can ablate tumors under many conditions (such as near-infrared thermogenesis, magnetocaloric effect or radioactivity). In general, magnetic nanomaterials need to be wrapped by hydrophilic inorganic substances to form the core of the microsphere, and the core-shell structure microsphere is formed by wrapping the polymer shell on the periphery through a series of reactions. However, using hydrophobic materials such as diallyl isophthalate to wrap magnetic nanoparticles has always been very challenging.

In this report, we propose a simple yet powerful method to synthesize polymeric magnetic microspheres. By the cation-π interaction, the benzene ring in the hydrophobic monomer DAIP reacts with Fe_3O_4 to form a hydrophobic magnetic fluid. One-step synthesis of embolized/magnetocaloric/imaging multifunctional microspheres can be realized by photopolymerization. This method is very rapid, which greatly reduces the synthesis time of microspheres. The inert allyl monomer in the thermal polymerization is activated by

irradiation now, and the reaction is very complete, which makes the purification of the microsphere simpler.

To verify the effect of the microspheres, we carried out a series of characterization compiling with *in vitro* and *in vivo* experiments. In the AMF, the temperature of the microsphere can reach 42–48°C, which can obviously inhibit the growth of tumor cells. In addition, we also studied the stability of the microspheres. In different kinds of solutions during the experiment, the particle size and heating performance of the microspheres remained the same, suggesting that the microspheres could be permanently embolized in vivo for a long time, and multiple-step operations could be avoided. Its imaging ability allows doctors and patients to monitor the position of microspheres and the progress of treatment during postoperative reexamination. This kind of magnetic microsphere with no obvious toxicity is valuable because it provides a direct and powerful one-step method to synthesize microspheres. It is an imaginable microsphere that can effectively inhibit tumor growth. However, this kind of microsphere also has its limitations, permanent embolization may cause hypoxia in the microenvironment, which is one of the causes of tumorigenesis. Another disadvantage is the uneven distribution of iron nanoparticles in the microspheres, which may lead to different heating effects. This will be proved in a further investigation. In a word, this method provides a reliable way to solve the problem that inorganic nano-magnetic materials cannot be well dispersed in hydrophobic monomers and have to rely on adsorption to form core-shell structure, which is generally requires stringent reaction conditions.

5. Conclusion

Based on the multi-allyl ether monomer, one-step photopolymerization was applied to produce Fe_3O_4@PDAIP magnetic microspheres successfully. Fe_3O_4@PDAIP magnetic microspheres not only achieve the different particle distribution clinically required for vessel obstruction, but also possess prominent heating and MRI enhanced signal ability with enough stability for a long-term embolization. All outstanding characteristics make Fe_3O_4@PDAIP magnetic microspheres an excellent candidate for tumor interventional therapy.

Abbreviations

AMF
Alternating magnetic field
HMPP
2-Hydroxy-2-methyl-1-phenyl-1-propanone
DAIP
Diallyl isophthalate
PVP
Polyvinyl pyrrolidone
PBS
Phosphate buffered saline

DMEM
Dulbecco's Modified Eagle Medium
FBS
Fetal bovine serum
IR
Infrared spectra
TG
Thermogravimetric
OD
optical densities
SEM
scanning electron microscopy
EDS
Energy Dispersive Spectrometer
CCK-8
cell counting kit-8

Declarations

Availability of data and materials

All data generated or analyzed during this study are included in this published article.

Acknowledgements

Not applicable.

Funding

This study was supported by the National Natural Science Foundation of China (Grant No. 21274032), the Natural Science Foundation of Guangdong Province (Grant No. 2014A030313500), and Science and Technology Projects in Guangzhou (Grant No. 202102080199).

Author's contribution

PC: Validation, Methodology, Software, Formal analysis, Data curation, Writing - Original Draft, Writing - Review & Editing, Visualization. **YZ**: Investigation, Methodology, Software, Data curation, Writing- Original draft preparation. **YL**: Validation. **QL**: Investigation. ***QX:*** Software. **YH:** Funding acquisition. **MC and JL:** Instrument support and technical guidance. **GY:** Conceptualization, Methodology, Software, Resources, Writing - Review & Editing, Supervision, Project administration, Funding acquisition.

Ethics declarations

Ethics approval and consent to participate

All animal procedures were performed under the guidelines of Intitutional Animal Care and Use Committee of Guangzhou Medical University.

Consent for publication

All authors agree to be published.

Competing interests

The authors declare that they have no competing interests.

References

1. Orron DE, Bloom AI, Neeman Z. The Role of Transcatheter Arterial Embolization in the Management of Nonvariceal Upper Gastrointestinal Bleeding. Gastrointest Endosc Clin N Am. 2018;28:331–49. doi:10.1016/j.giec.2018.02.006.
2. Oishi Y, Tani K, Ozono K, Itamoto K, Haraguchi T, Taura Y. Transcatheter arterial embolization in normal canine liver. Vet Surg. 2017;46:797–802. doi:10.1111/vsu.12663.
3. Shimohira M, Hashizume T, Sasaki S, Ohta K, Suzuki K, Nakagawa M, Ozawa Y, Sakurai K, Nishikawa H, Hara M. Transcatheter Arterial Embolization for Hepatic Arterial Injury Related to Percutaneous Transhepatic Portal Intervention. Cardiovasc Inter Rad. 2017;40:291–5. doi:10.1007/s00270-016-1471-6.
4. Park TG, Lu W, Crotts G. Importance of in vitro experimental conditions on protein release kinetics, stability and polymer degradation in protein encapsulated poly (d, l-lactic acid-co-glycolic acid) microspheres. J Control Release. 1995;33:211–22. doi:10.1016/0168-3659(94)00084-8.
5. Shameem M, Lee H, DeLuca PP. A short term (accelerated release) approach to evaluate peptide release from PLGA depot-formulations. AAPS PharmSci. 1999;1:E7. doi:10.1208/ps010307.
6. Shen J, Burgess DJ. Accelerated in-vitro release testing methods for extended-release parenteral dosage forms. J Pharm Pharmacol. 2012;64:986–96. doi:10.1111/j.2042-7158.2012.01482.x.
7. Salem R, Gordon AC, Mouli S, Hickey R, Kallini J, Gabr A, Mulcahy MF, Baker T, Abecassis M, Miller FH, Yaghmai V, Sato K, Desai K, Thornburg B, Benson AB, Rademaker A, Ganger D, Kulik L, Lewandowski RJ Y90 Radioembolization Significantly Prolongs Time to Progression Compared With Chemoembolization in Patients With Hepatocellular Carcinoma. *Gastroenterology* 2016, 151, 1155–1163.e2. doi:10.1053/j.gastro.2016.08.029 **2016**.
8. Lee EW, Thakor AS, Tafti BA, Liu DM. Y90 Selective Internal Radiation Therapy. Surg Oncol Clin N Am. 2015;24:167–85. doi:10.1016/j.soc.2014.09.011.
9. Saini A, Wallace A, Alzubaidi S, Knuttinen MG, Naidu S, Sheth R, Albadawi H, Oklu R. History and Evolution of Yttrium-90 Radioembolization for Hepatocellular Carcinoma. J Clin Med. 2019;8:55.

doi:10.3390/jcm8010055.

10. Yang W, Guo W, Le W, Lv G, Zhang F, Shi L, Wang X, Wang J, Wang S, Chang J. Albumin-Bioinspired Gd:CuS Nanotheranostic Agent for In Vivo Photoacoustic/Magnetic Resonance Imaging-Guided Tumor-Targeted Photothermal Therapy. ACS Nano. 2016;10:10245–57. doi:10.1021/acsnano.6b05760.
11. Kam NW, O'Connell M, Wisdom JA, Dai H. Carbon nanotubes as multifunctional biological transporters and near-infrared agents for selective cancer cell destruction. Proc Natl Acad Sci U S A. 2005;102:11600–5. doi:10.1073/pnas.0502680102.
12. O'Neal DP, Hirsch LR, Halas NJ, Payne JD, West JL. Photo-thermal tumor ablation in mice using near infrared-absorbing nanoparticles. Cancer Lett. 2004;209:171–6. doi:10.1016/j.canlet.2004.02.004.
13. Li L, Guo X, Peng X, Zhang H, Liu Y, Li H, He X, Shi D, Xiong B, Zhao Y. Radiofrequency-responsive dual-valent gold nanoclusters for enhancing synergistic therapy of tumor ablation and artery embolization. Nano Today. 2020;35:100934. doi:10.1016/j.nantod.2020.100934.
14. Lee EW, Alanis L, Cho S, Saab S. Yttrium-90 Selective Internal Radiation Therapy with Glass Microspheres for Hepatocellular Carcinoma: Current and Updated Literature Review. Korean J Radiol. 2016;17:472. doi:10.3348/kjr.2016.17.4.472.
15. Hsieh T, Hung P, Wang C, Tso K, Wang H, Cheng C, Lin Y, Chung R, Wei K, Wu P, et al. Synthesis of IrO_2 decorated core–shell PS@PPyNH$_2$ microspheres for bio-interface application. Nanotechnology. 2020;31:375605. doi:10.1088/1361-6528/ab9678.
16. Xu C, Pu K. Second near-infrared photothermal materials for combinational nanotheranostics. Chem Soc Rev. 2021;50:1111–37. doi:10.1039/D0CS00664E.
17. Wang H, Pu X, Zhou Y, Chen X, Liao X, Huang Z, Yin G Synthesis of Macroporous Magnetic Fe_3O_4 Microparticles Via a Novel Organic Matter Assisted Open-Cell Hollow Sphere Assembly Method. *Materials* 2018, 11, 1508, doi:10.3390/ma11091508.
18. Jiang F, Ding B, Zhao Y, Liang S, Cheng Z, Xing B, Teng B, Ma PA, Lin J. Biocompatible CuO-decorated carbon nanoplatforms for multiplexed imaging and enhanced antitumor efficacy via combined photothermal therapy/chemodynamic therapy/chemotherapy. Sci China Mater. 2020;63:1818–30. doi:10.1007/s40843-019-1397-0.
19. Fan M, Jiang M. Core-shell nanotherapeutics with leukocyte membrane camouflage for biomedical applications. J Drug Target. 2020;28:873–81. doi:10.1080/1061186X.2020.1757102.
20. Ma X, Li Y, Hussain I, Shen R, Yang G, Zhang K. Core–Shell Structured Nanoenergetic Materials: Preparation and Fundamental Properties. Adv Mater. 2020;32:2001291. doi:10.1002/adma.202001291.
21. Chou P, Lin F, Hsu H, Chang C, Lu C, Chen J. Electrorheological Sensor Encapsulating Microsphere Media for Plague Diagnosis with Rapid Visualization. Acs Sens. 2020;5:665–73. doi:10.1021/acssensors.9b01529.

22. Zhang Y, Huang H, Liang Z, Liu H, Yi L, Zhang J, Zhang Z, Zhong C, Huang Y, Ye G. Microscopic progression in the free radical addition reaction: modeling, geometry, energy, and kinetics. J Mol Model 2017, 23, doi:10.1007/s00894-017-3217-z.
23. Zhao X, Huang W, Lin S, Chen X, Guo X, Zou D, Ye G. Density Functional Theory Guide for an Allyl Monomer Polymerization Mechanism: Photoinduced Radical-Mediated [3 + 2] Cyclization. ACS Omega. 2021;6:15608–16. doi:10.1021/acsomega.1c00165.
24. Zhao X, Huang W, Li X, Lin R, Li Q, Wu J, Yu Z, Zhou Y, Huang H, Yu M, et al. One-step preparation of photoclick method for embolic microsphere synthesis and assessment for transcatheter arterial embolization. Eur J Pharm Biopharm. 2021;166:94–102. doi:10.1016/j.ejpb.2021.06.002.
25. Murthy NS, Zhang Z, Borsadia S. Nanospheres with a smectic hydrophobic core and an amorphous PEG hydrophilic shell: Structural changes and implications for drug delivery. Soft Matter. 2018;21:1327–35. doi:10.1039/c7sm02472.
26. Bhattacharyya PK. Exploring Cation – π Interaction in the Complexes with B ≡ B Triple Bond: A DFT Study. J Phys Chem A. 2017;121:3287–98. doi:10.1021/acs.jpca.7b01326.
27. Dougherty DA. The Cation – π Interaction. Acc Chem Res. 2013;46:885–93. doi:10.1021/ar300265y.
28. Demircan ÇA, Bozkaya U. Transition Metal Cation – π Interactions: Complexes Formed by Fe^{2+}, Co^{2+}, Ni^{2+}, Cu^{2+}, and Zn^{2+} Binding with Benzene Molecules. J Phys Chem A. 2017;121:6500–9. doi:10.1021/acs.jpca.7b05759.
29. Qiu J, Zhang T, Zhu X, Yang C, Wang Y, Zhou N, Ju B, Zhou T, Deng G, Qiu C. Hyperoside Induces Breast Cancer Cells Apoptosis via ROS-Mediated NF-κB Signaling Pathway. Int J Mol Sci. 2020;21:131. doi:10.3390/ijms21010131.
30. Meng Xu. Y.W.Y.L. Hollow mesoporous ruthenium nanoparticles conjugated bispecific antibody for targeted anti-colorectal cancer response of combination therapy. Nanoscale. 2019;11:9661–78. doi:10.1039/c9nr01904a.
31. Li S, Sun Y, Tian T, Qin X, Lin S, Zhang T, Zhang Q, Zhou M, Zhang X, Zhou Y, et al. MicroRNA-214-3p modified tetrahedral framework nucleic acids target survivin to induce tumour cell apoptosis. Cell Proliferat 2020, 53, doi:10.1111/cpr.12708.
32. Fowler KJ, Maughan NM, Laforest R, Saad NE, Sharma A, Olsen J, Speirs CK, Parikh P. J. PET/MRI of Hepatic 90Y Microsphere Deposition Determines Individual Tumor Response. Cardiovasc Inter Rad. 2016;39:855–64. doi:10.1007/s00270-015-1285-y.
33. Chen J, Guo J, Chen Z, Wang J, Liu M, Pang X. Linifanib (ABT-869) Potentiates the Efficacy of Chemotherapeutic Agents through the Suppression of Receptor Tyrosine Kinase-Mediated AKT/mTOR Signaling Pathways in Gastric Cancer. Sci Rep-Uk 2016, 6, doi:10.1038/srep29382.
34. Dreher MR, Sharma KV, Woods DL, Reddy G, Tang Y, Pritchard WF, Chiesa OA, Karanian JW, Esparza JA, Donahue D, Levy EB, Willis SL, Lewis AL, Wood BJ. Radiopaque drug-eluting beads for transcatheter embolotherapy: experimental study of drug penetration and coverage in swine. J Vasc Interv Radiol. 2012;23(2):257 – 64.e4. doi:10.1016/j.jvir.2011.10.019.

35. Zhao Y, Chen T, Sun S, Zhao L. Preparation of Magnetic Hybrid Microspheres with Well-Defined Yolk-Shell Structure. Adv Mater Sci Eng. 2016;2016:1–7. doi:10.1155/2016/2658621.
36. Cao XL, Cheng C, Ma YL, Zhao CS. Preparation of silver nanoparticles with antimicrobial activities and the researches of their biocompatibilities. J Mater Science: Mater Med. 2010;21:2861–8. doi:10.1007/s10856-010-4133-2.
37. PARK H, JO S, CHO H, JUNG U. Synergistic Anti-cancer Activity of MH-30 in a Murine Melanoma Model Treated With Cisplatin and its Alleviated Effects Against Cisplatin-induced Toxicity in Mice. *In* Vivo. 2020;34:1845–56. doi:10.21873/invivo.11979.
38. Wei Y, Wang D, Chen M, Ouyang Z, Wang S, Gu J. Extrahepatic cytochrome P450s play an insignificant role in triptolide-induced toxicity. Chin Med-Uk 2018, 13, doi:10.1186/s13020-018-0179-8.

Schemes

Schemes 1 is available in the Supplementary Files section

Figures

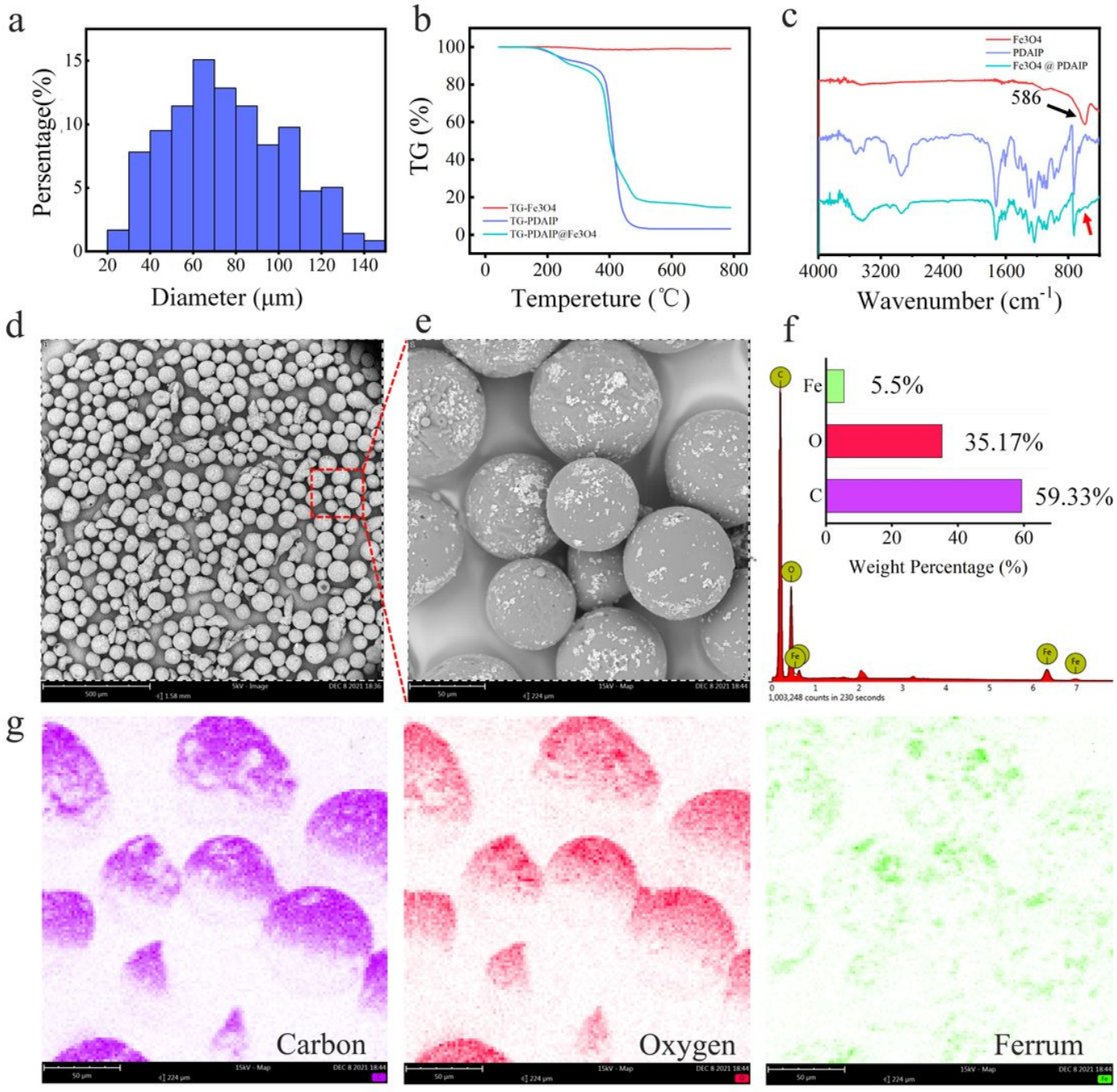

Figure 1

Morphological characterization, spectral analysis and elemental analysis of magnetic microsphere. (a) Particle size distribution of microsphere; (b) TG curve of thermal analysis; (c) Infrared spectroscopy curve; (d) Overview of microspheres at low magnification in SEM; (e) Enlarged view of the box-selected part in d part; (f) Full-range elemental analysis of e part; (g) The corresponding elemental mapping images (C, O and Fe) of Fe_3O_4@PDAIP magnetic microspheres in g part.

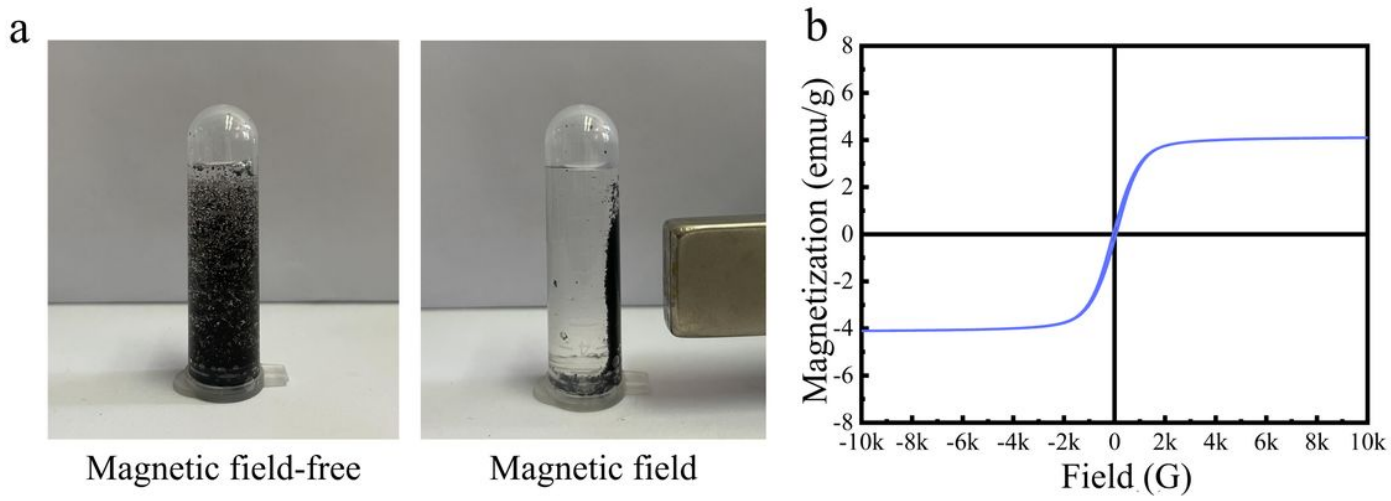

Figure 2

Magnetic test of Fe_3O_4@PDAIP magnetic microspheres. (a) Microspheres without and with a magnet; (b) Magnetic response intensity of microspheres (30.44mg).

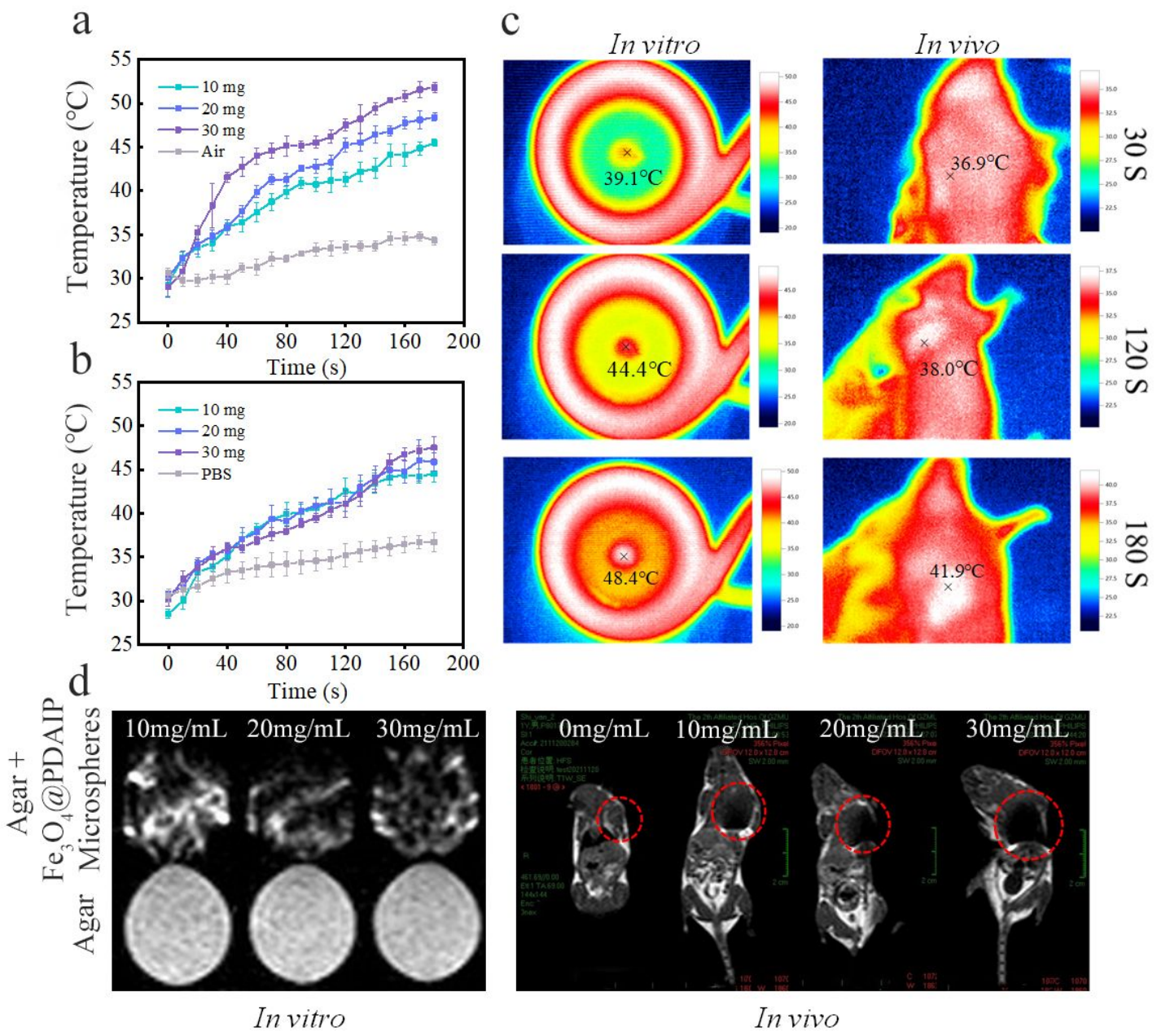

Figure 3

Heating and MRI imaging of Fe_3O_4@PDAIP magnetic microspheres in vitro and in vivo. (a) Temperature changes of different doses of microspheres in AMF without cells; (b) Temperature changes of different doses of microspheres in AMF with cells; (c) Temperature rising process of microspheres in AMF (The 30mg/mL microspheres are located in the center of coil). (d) MRI imaging ability of microspheres (The upper is the mixture of microspheres and agar, and the lower is the control group: pure agar without microspheres).

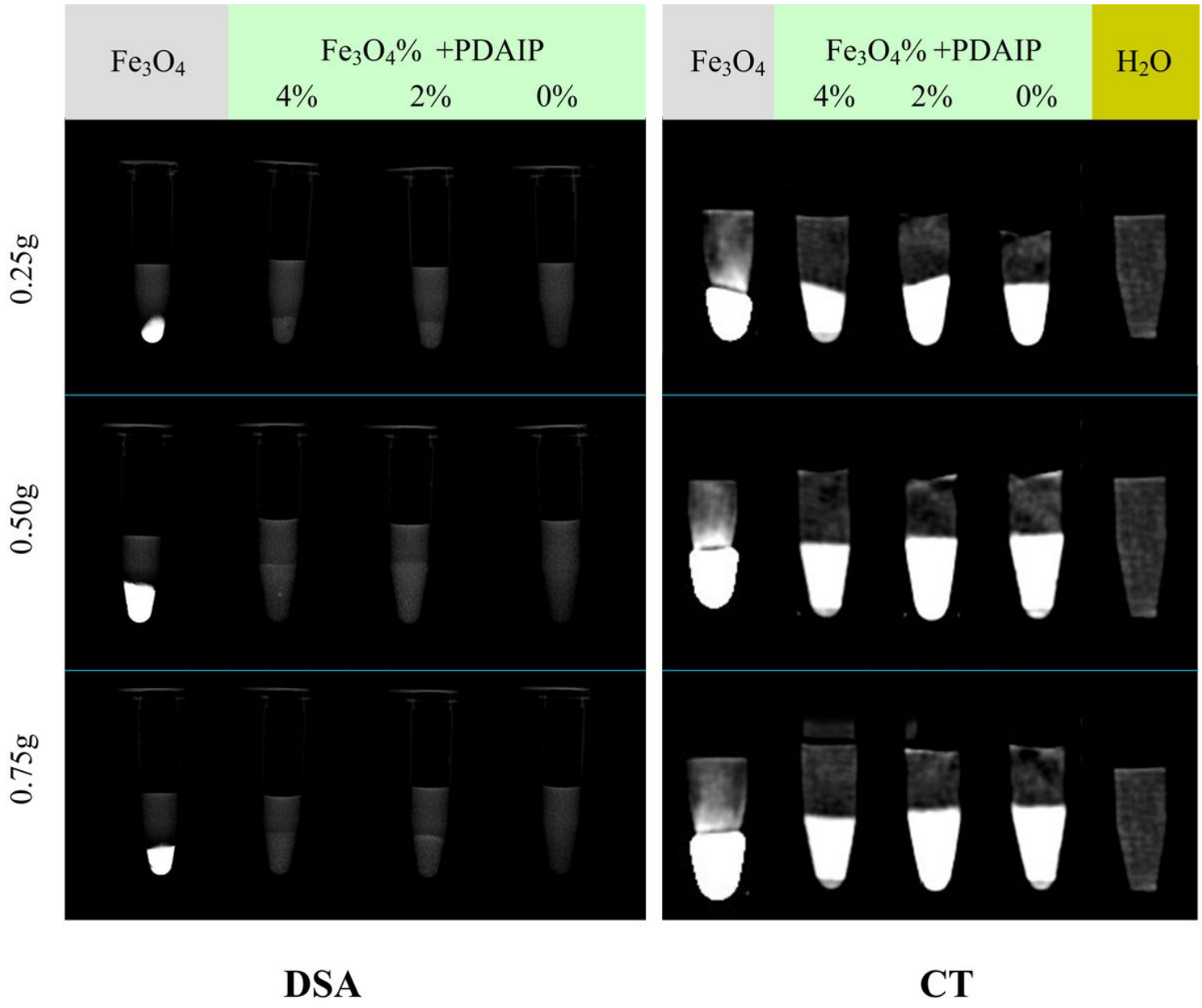

Figure 4

DSA and CT imaging of Fe_3O_4@PDAIP.

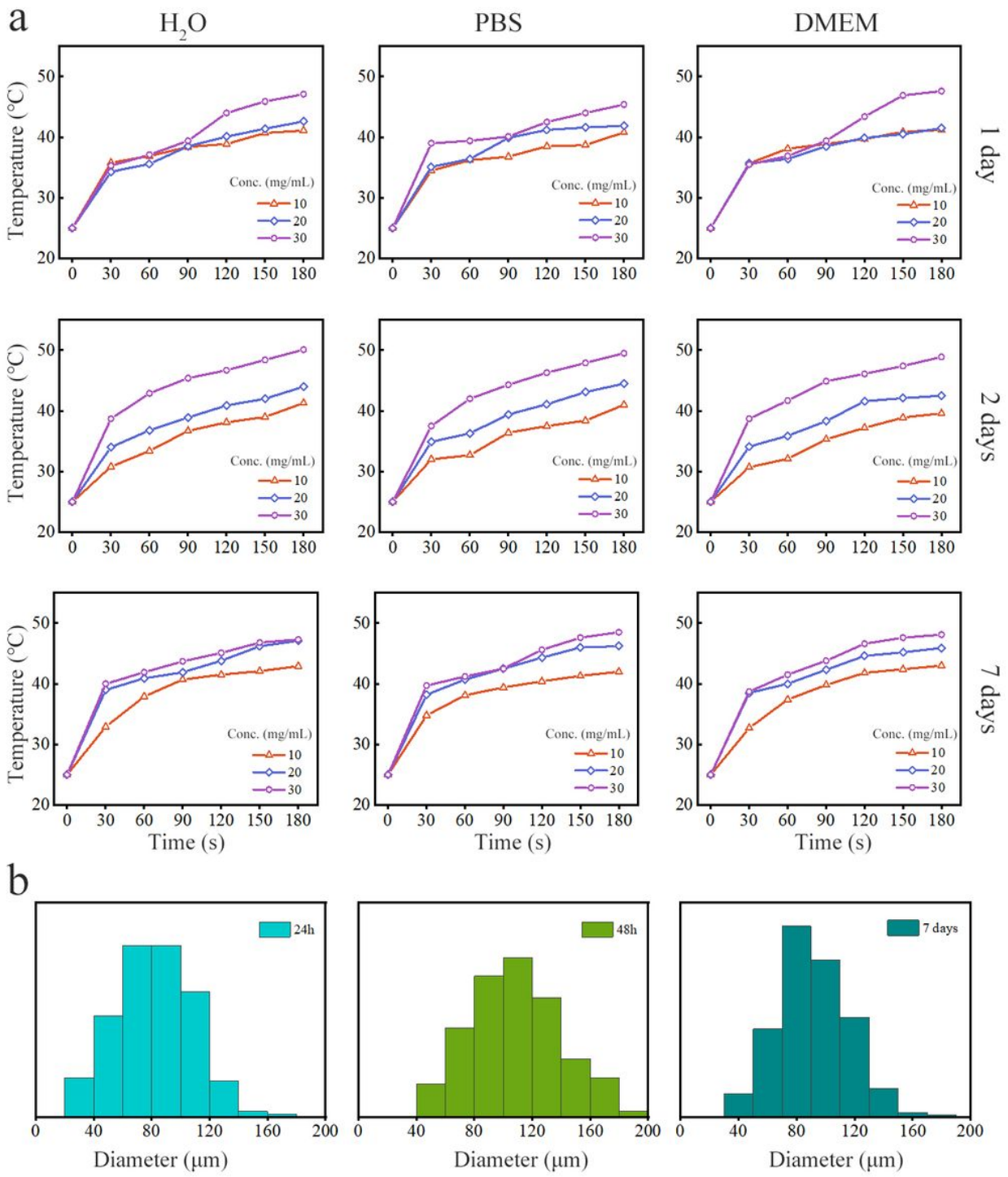

Figure 5

Stability of Fe_3O_4@PDAIP magnetic microspheres after soaking in H_2O, PBS and DMEM for 1, 2 and 7 days, respectively. (a) Heating performance (b) Particle size distribution.

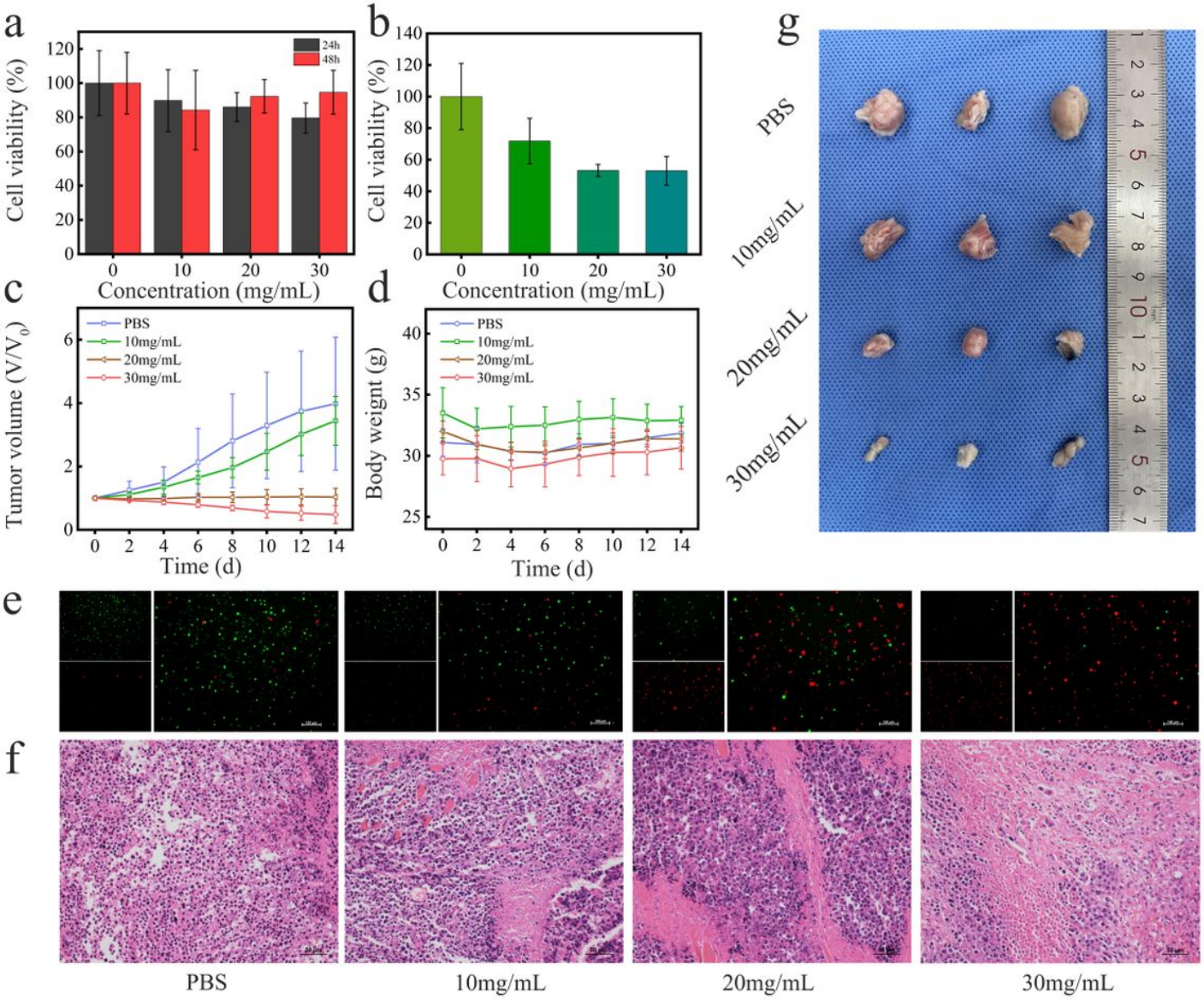

Figure 6

Anti-tumor experiment of different concentrations Fe_3O_4@PDAIP magnetic microspheres *in vitro* and *in vivo*. (a) The relative cell viability within 1 or 2 days in different concentrations of microspheres. (b) Relative cell viability in AMF for 180s. (c) Relative tumor volume after treatment in AMF within 14 days. (d) Body weight record of mice within 14 days. (e) Fluorescent staining of live (green) and dead (red) cell. (f) H&E staining of tumor tissue with Fe_3O_4@PDAIP microspheres. (g) The size of solid tumor on the 14th day after treatment.

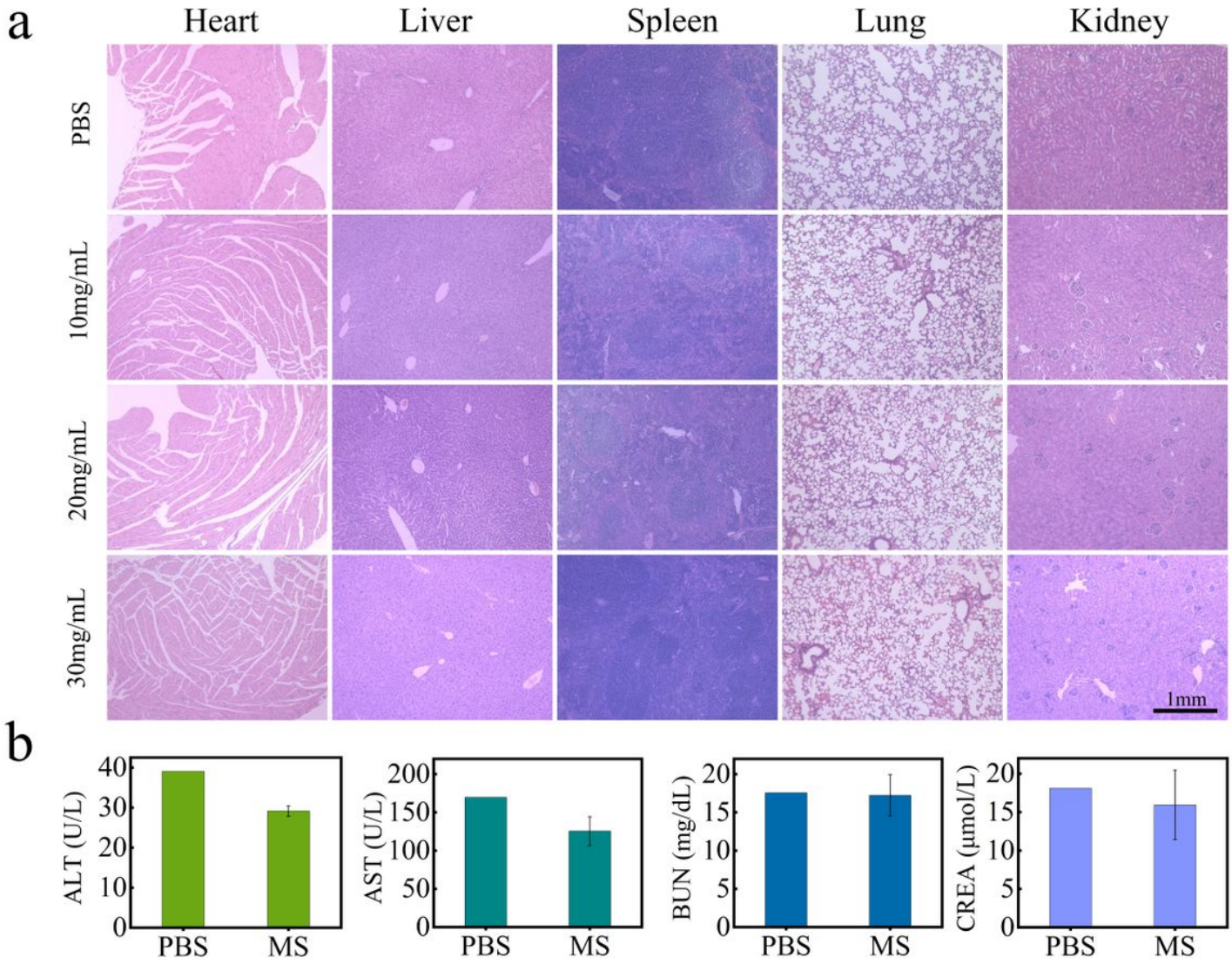

Figure 7

Histopathological examination and serum detection. (a) Histopathological sections of heart, liver, spleen, lung and kidney after treatment with different concentrations of microspheres; (b) Serum test results including ALT and AST as indicators of liver function, while BUN and CREA as indicators of renal function.

Supplementary Files

This is a list of supplementary files associated with this preprint. Click to download.

- TOC.jpg
- Scheme1.SynthesisofFe3O4PDAIPmagneticmicrospheres.jpg